Design of Non-Uniform Metasurface-Based Phased-Array Antenna for Grating Lobes Mitigation

Samuel Nsimba Lubanzu
Department of Electrical Engineering (Telecommunication Option), Pan African University, Institute for Basic Sciences, Technology and Innovation (PAUSTI), Nairobi, Kenya
nlubanzu@gmail.com (corresponding author)

Dominic Bernard Onyango Konditi
School of Electrical and Electronics Engineering, Technical University of Kenya (TUK), Nairobi, Kenya
konditidbo@gmail.com

Philip Kibet Langat
Jomo Kenyatta University of Agriculture and Technology, Nairobi, Kenya
kibetlp@jkuat.ac.ke

Received: 17 July 2025 | Revised: 18 August 2025 | Accepted: 2 September 2025

 DOI: https://doi.org/10.48084/etasr.13471

ABSTRACT

Grating lobes pose significant limitations to antenna array directivity and radiation efficiency, affecting the performance of wireless communication systems. This paper introduces a novel 2 × 2 phased microstrip patch antenna array integrated with a non-uniform metasurface acting as a Partially Reflective Surface (PRS) for grating lobe suppression. The non-uniform metasurface, composed of 11 × 11 unit cells, is placed above the array to form a Fabry–Perot Cavity (FPC), enabling constructive interference in the main beam direction and attenuation of undesired lobes. The non-uniform metasurface design, inspired by current-density tapering, offers a novel approach to grating-lobe problems. With an element spacing of $1.04\lambda_0$ at 12.5 GHz, rigorous design optimization shows Grating Lobe Levels (GLLs) of -20.22 dB and peak gain increases from 10.3 dB to 19.1 dB, highlighting the design's effectiveness. This design offers a simple, low-profile solution for 5G base stations, radar, and satellite applications.

Keywords-non-uniform metasurface; grating-lobe suppression; current-density taper; 5G applications

I. INTRODUCTION

The array antenna is an indispensable component of an antenna system, as it provides significant advantages, including enhanced gain and directivity, improved signal strength, efficient power usage, and the ability to focus energy in a specific direction. The applications of phased arrays in modern wireless communication systems include sensing-based automotive radar, anti-collision radar, smart cities, and satellite communications, among others. Phased array antennas are composed of numerous fixed antenna elements that are configured to form an effective main lobe [1, 2]. By manipulating the phase of each element, the radiation pattern of a phased array can be controlled in a specific direction, whereas radiations in unwanted directions can be suppressed. Thus, the overall array performance, including the directivity and the gain, depends on the radiation properties of each element in the antenna array [3]. In phased array design, one-wavelength element spacing is often preferred because it provides a balance between overall performance and practicability [4]. This choice is justified by the reduced number of elements required and low complexity. However, when the spacing between the elements in the array is greater than half the wavelength of the signal, lobes other than the main lobe appear. These are called grating lobes, which significantly impact the directivity and gain, limiting the overall array performance.

Many solutions have been proposed to enhance the radiation pattern and reduce grating lobes that appear in phased arrays with large element spacing. Methods based on array configuration have been widely applied to cancel grating lobes [1, 4-6]. One involves employing non-uniform or triangular-latticed element distributions from the perspective of the array factor, whereas the other revolves around the element pattern aspect and entails the use of antenna elements with pattern nulls precisely positioned at the grating-lobe directions [7, 8]. However, this technique results in efficiency loss. Grating

lobes can also be avoided by randomizing the distribution of elements, which disrupts the periodicity of the array and limits in-phase overlap. This method considers a large number of periodic, non-uniform subarrays or phased arrays, which requires complex optimization algorithms and large computational resources to effectively reduce grating lobes. Recent research has investigated various implementations of Partially Reflective Surfaces (PRS) and Frequency Selective Surfaces (FSS) for grating-lobe mitigation [9, 10]. A double-sided PRS was utilized in [9] to mitigate the radiation pattern of a 2 × 2 electrically large antenna array with $1.47\lambda_0$ element separation and sustain the TM_{30} mode. Although it improved the main beam, there was some efficiency loss, and only a –15.5 dB Grating Lobe Level (GLL) was achieved. To address the impact of diffracted fields caused by grating lobes, authors in [11] incorporated an Artificial Magnetic Conductor (AMC) side and central walls with a Fabry-Pérot Cavity (FPC), resulting in improved distribution uniformity and grating-lobe reduction at the cost of a bulky structure. Similarly, the work in [12] utilized a PRS with a non-standard AMC reflective ground plane in an FPC resonator antenna fed by a linearly polarized source. The work in [13] utilized a PRS-based thinned array concept using Printed Circuit Board (PCB) technology to cancel the grating lobes. Further, dielectric superlayers with a higher permittivity were incorporated in [14] to mitigate arrays with large periodicity from grating lobes. A multilayer FSS was used in [10] and achieved a –10 dB grating-lobe reduction, but resulted in a bulky and complex design.

Among various applications, the use of metasurfaces has emerged as a promising technique for improving antenna performance. Incorporating metasurfaces into antenna structures presents a significant advantage, as it improves gain and enables low-profile antennas [15], reduces coupling effects between adjacent antenna elements, and enhances directivity, whereas it mitigates grating lobes by controlling the propagation of electromagnetic waves [16-18]. This method, however, often requires complex optimization or large apertures. In [18], a metasurface lens was used over a planar antenna array for grating-lobe suppression, and high performance was achieved at the cost of increased volume. When a metasurface is used as PRS placed above antenna arrays, a compact and simple structure is obtained by forming an FPC that constructively reinforces the main beam and suppresses grating lobes [9]. This approach often suffers from efficiency loss, large multilayer structures, or complicated optimization problems. A non-uniform metasurface offers a simple method to control the radiation beam of antennas. For example, authors in [19] used a non-uniform metasurface lens for gain improvement and main-beam focusing. Several studies have explored metasurface, however, the potential of a compact, single-layer non-uniform metasurface for effective and low-complexity grating-lobe mitigation in phased arrays is still under active research.

We introduce a new 2 × 2 phased microstrip antenna array with a non-uniform metasurface-based PRS under an FPC configuration that provides a low-profile and efficient solution for grating-lobe suppression. Unlike existing approaches, the proposed design eliminates the need for complex algorithms or bulky multilayer structures. Full-wave simulations show a minimum GLL of –20.22 dB and a peak gain of 19.1 dB at 12.5 GHz, outperforming previous designs using FPCs. A sensitivity analysis further demonstrates that the design is robust and suitable for implementation in real systems, such as 5G base stations, radar, and satellites.

II. THEORETICAL BACKGROUND AND PROPOSED GRATING-LOBE MITIGATION TECHNIQUE

Grating lobes appear in radiation patterns as undesired radiation at angles other than the main beam, occurring when there is a large spacing between elements [3]. In antenna radiation patterns, grating lobes result from periodic antenna array structures. This phenomenon significantly diminishes radiation efficiency and the ability to focus signals. According to antenna array theory, grating lobes are avoided when the element spacing in an array satisfies the condition:

$$dx, dy \leq \frac{\lambda}{1+|\sin(\theta)|} \quad (1)$$

where dx , dy are the element spacings in a planar configuration, λ is the operating wavelength in free space, and θ is the direction of the main beam. In this study, we consider a fixed beam at broadside. According to (1), a straightforward solution to completely mitigate grating lobes involves reducing the inter-element distance to less than $0.5\lambda_0$. However, when the spacing between elements is reduced, mutual coupling effects become pronounced, resulting in gain degradation and a distorted radiation pattern. An alternative is to use a metasurface to control wavefronts and phase responses, enabling grating-lobe suppression in the radiation pattern [20-22]. The proposed design workflow for grating-lobe reduction is summarized as follows:

- A planar array with large element spacing and unavoidable grating lobes was designed to serve as a baseline.
- The amplitude and phase of the metasurface were tailored to be used as a PRS for improving the radiation characteristics of the phased array.
- The effect of the metasurface placed on top of the antenna array was analyzed under different conditions to obtain optimal characteristics.
- Using recorded current density on the metasurface, a non-uniform metasurface was formed to further reduce grating lobes.

III. METHODOLOGY

A. Antenna Array Design

The designed antenna is a planar 2 x 2 array composed of microstrip patches backed by a full ground plane, printed on FR4 substrate with permittivity (ε_r) of 4.4, a loss tangent of 0.02, and a thickness (t) of 1.5 mm. We first designed a single element, and a wave port was used for excitation to analyze its performance at the desired operating frequency of 12.5 GHz. Figure 1(a) shows the basic structure of a single element. Each element is fed individually by probe feed for easy impedance matching (Figure 1(b)). Rectangular microstrip patches were employed for their flexibility to be optimized for a directive pattern.

The unit element antenna was designed to operate at 12.5 GHz. For a microstrip patch antenna, the width (W) and the length (L) of the patch can be obtained as follows [3]:

$$W = \frac{\lambda_0}{2\sqrt{0.5(\varepsilon_r+1)}} \quad (2)$$

$$L = \frac{\lambda_0}{2\sqrt{\varepsilon_{eff}}} \quad (3)$$

where λ_0 denotes the operating wavelength andε_r is the relative primitivity of the substrate. In (3), ε_{eff} represents the effective permittivity, which varies with the width of the patch (W) and the thickness (t) of the substrate, and can be calculated as:

$$\varepsilon_{eff} = \frac{\varepsilon_r+1}{2} + \frac{\varepsilon_r+1}{2}\left(\frac{1}{\sqrt{1+\frac{12t}{w}}}\right)^{-0.5} \quad (4)$$

Taking into account the fringing fields effect that affect the beam direction and side-lobe levels, the length of the patch:

$$L_{eff} = L - 2\Delta L \quad (5)$$

$$\Delta L = 0.412t \times \left[\frac{(\varepsilon_{eff}+0.3)\left(\frac{w}{t}+0.264\right)}{\varepsilon_{eff}-0.258\left(\frac{w}{t}+0.813\right)}\right] \quad (6)$$

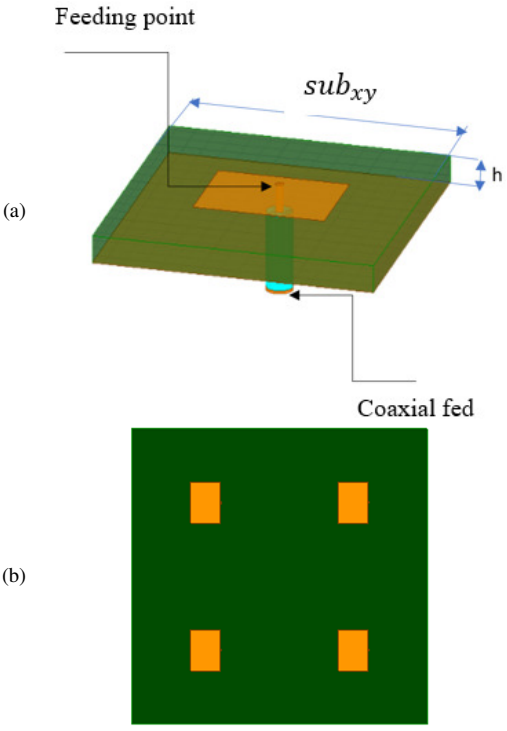

Fig. 1. (a) Single antenna element structure, (b) 2 × 2 array configuration.

From numerical calculations, the width and length of the radiating patch were determined to be 7.6 mm and 5.3 mm, respectively. To ensure a uniform radiation pattern and minimal mutual coupling, the ground plane size was designed to be similar to the substrate and larger than the radiating element. The substrate was set to a square of 25 mm, which corresponds to $1.04\lambda_0$ at 12.5 GHz. These values were adjusted through extensive parameter sweeps to obtain better impedance matching and maintain good radiation performance. The optimized parameters were $w_{opt} = 7$ mm, $L_{opt} = 5$ mm, and $y_0 = 2.5$ mm. All the simulations were carried out using the High-Frequency Structure Simulator (HFSS). The unit elements were then placed together to form a 2 × 2 antenna array with an element spacing of $1.04\lambda_0$. The simulated S-parameters, depicted in Figure 2(a), show that the impedance bandwidth is below -10 dB from 12 GHz to 13.2 GHz. As predicted by (1) and observed in Figure 2(b), an element spacing of $1.04\lambda_0$ introduces a grating lobe of −6 dB (at 60°) in the first quadrant of the radiation pattern.

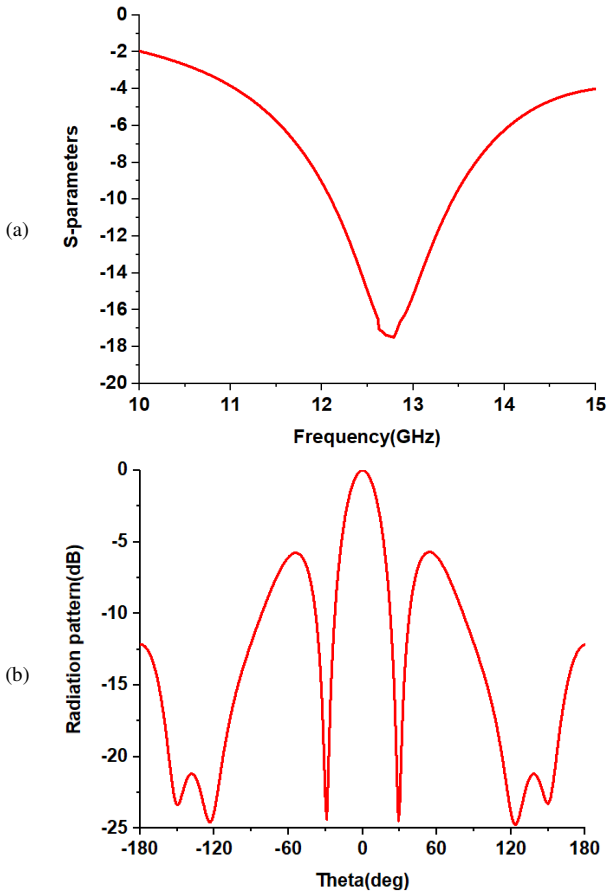

Fig. 2. Simulated characteristics of the antenna array for an element spacing of 25 mm: (a) S-parameters, (b) radiation pattern.

B. Unit Cell Design

The structure of the unit cell is depicted in Figure 3(a). Each unit cell is composed of a 6.75 × 6.75 mm^2 square metal layer made from copper. In contrast to the structure suggested in [9], a single dielectric layer is used on one side to form the unit cell. A low-loss dielectric layer with a periodicity (p) of 8 mm was utilized. The substrate is Rogers 5880, with a thickness of 0.787 mm, a relative permittivity of 2.2, and a dielectric loss of 0.0009, which enhances the fields leaking through the superstrate. Each unit cell was analyzed using master–slave boundaries and Floquet ports, as shown in Figure 3(b). The master and slave boundaries were set along the x- and

y-directions, whereas Floquet ports were applied along the z-direction. The simulation was performed using HFSS, a full wave simulation tool based on the Finite Element Method (FEM).

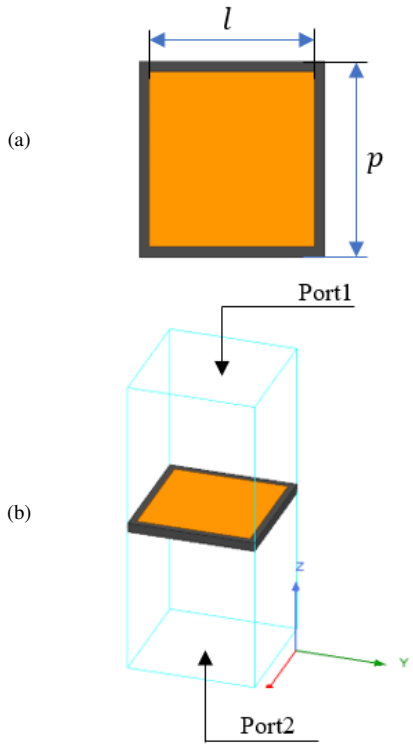

Fig. 3. (a) Geometry of the unit cell, (b) analysis setup of the unit cell.

As shown in Figure 4(a), the reflection amplitude of the unit cell within the operating bandwidth ranges from 0.86 to 0.88. This reflection coefficient enables a balance between reflection and transmission, enhancing the resonant cavity effect, which increases the gain and reduce grating lobes. Meanwhile, a reflection phase of −152° is obtained across the bandwidth, as shown Figure 4(b). This phase shift, being close to −180° (out-of-phase), facilitates constructive interference in the boresight direction when the metasurface is spaced appropriately at $\lambda_0/2$ (at 12.5 GHz) above the array. This configuration increases the gain and directivity by narrowing the main lobe and reducing grating lobes. The effect of these values will be further discussed in the next section.

C. Antenna Array with Metasurface

The proposed structure of the antenna array integrated with the metasurface is shown in Figure 5. The metasurface is composed of 11 × 11 unit cells and is located on top of the feeding antenna, acting as an inductive PRS. The overall size of the metasurface is 110 × 110 mm^2. The size of the metasurface was carefully determined to effectively enhance directivity by improving phase coherence, to minimize sidelobes, and to achieve higher gain and efficiency. To match the metasurface dimensions, the antenna array aperture was extended to 110 × 110 mm^2, to ensure consistent interaction between the radiated fields and the metasurface.

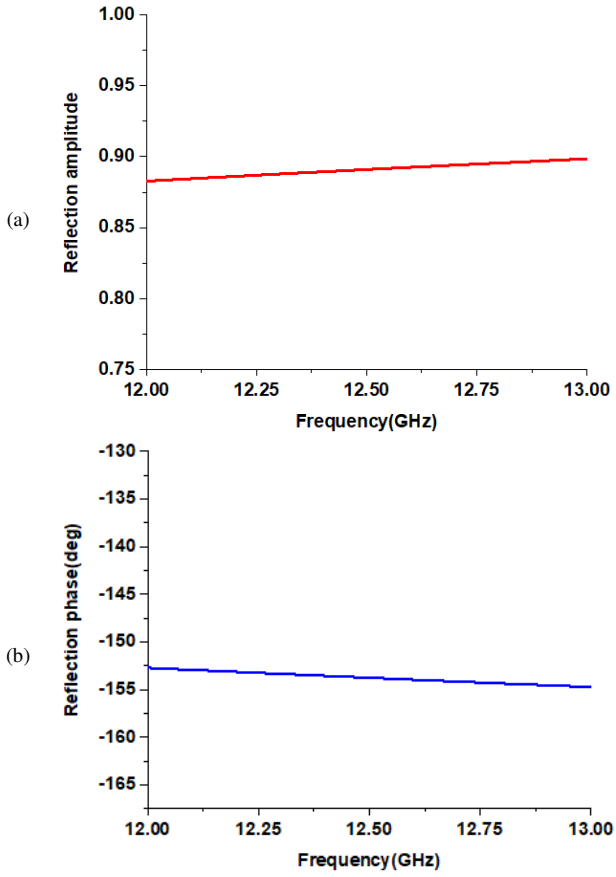

Fig. 4. Characteristics of the unit cell: (a) reflection amplitude, (b) reflection phase.

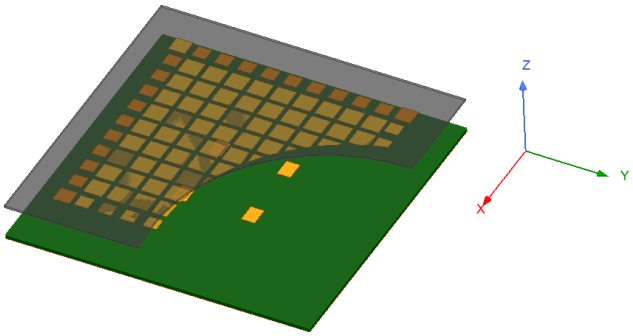

Fig. 5. Overall view of the proposed 4 × 4 antenna array with metasurface.

An FPC antenna operates by placing a PRS above a radiating antenna to form a resonant cavity. Electromagnetic waves emitted from the antenna undergo multiple reflections between the PRS and the ground plane, causing constructive interference that enhances the main beam directivity and gain while suppressing unwanted lobes. When an electromagnetic wave interacts with a conducting surface, such as a metallic patch, it induces surface currents within the conductor [23]. These currents, in turn, produce secondary electromagnetic fields that influence the incident wave. Thus, the grating lobes produced by the feeding antenna can be reduced by controlling the currents on the metasurface.

The directivity can be expressed as a function of the complex reflection coefficient of the superstrate [9]:

$$D_{max} = \frac{1+\left|Re^{j\varphi_{prs}}\right|}{1-\left|Re^{j\varphi_{prs}}\right|} \quad (7)$$

And the thickness (H) of the air cavity is given by:

$$H = \frac{\lambda_0}{4\pi}\left(\varphi_{prs} + \varphi_{gnd} - 2n\pi\right), n = 0, 1, 2, \ldots \quad (8)$$

where R is the complex reflection coefficients of the PRS and φ_{gnd} is the reflection phase of the ground plane. The ground plane is assigned as a perfect electric conductor, providing a maximum reflection phase when $\varphi_{gnd} = \pi$. To obtain a low profile, the first resonance ($n = 0$) was chosen, corresponding to $H = 0.5\lambda_0$ at 12.5 GHz.

IV. PERFORMANCE EVALUATION

A. *Effect of Unit Cell Element Spacing*

Figure 6 depicts the radiation pattern of the antenna array integrated with the metasurface. The performance of the overall structure was analyzed with different unit cell element spacings from center to center, ranging from 7.75 mm to 10.75 mm, whereas all other design parameters were kept unchanged. It was observed that the grating-lobe level can be controlled by adjusting the spacing between unit cells. When the distance between unit cells ranges from 7.75 mm to 8.25 mm, a minimal grating lobe of –18.5 dB is achieved. This is due to the capacitive effect between the elements of the metasurface.

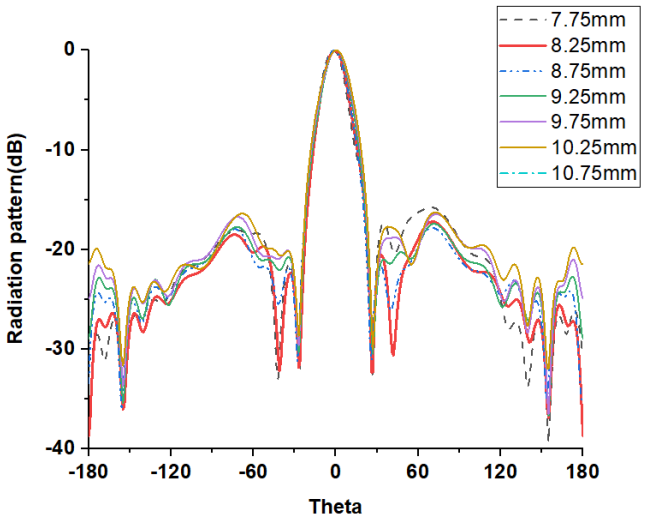

Fig. 6. Radiation pattern with different unit cell element spacings.

B. *Effect of Cavity Height*

A parametric sweep was conducted to identify the optimal cavity thickness for the FPC antenna. The analysis confirmed low grating-lobe levels (–18.5 dB) at a cavity height (H) of 13 mm, as shown in Figure 7. This optimized thickness, combined with precise determination of the unit cell element spacing in the PRS, resulted in a gain of 17.5 dB at 12.5 GHz, enhancing the antenna's overall efficiency and directivity at the given frequency (Figure 8).

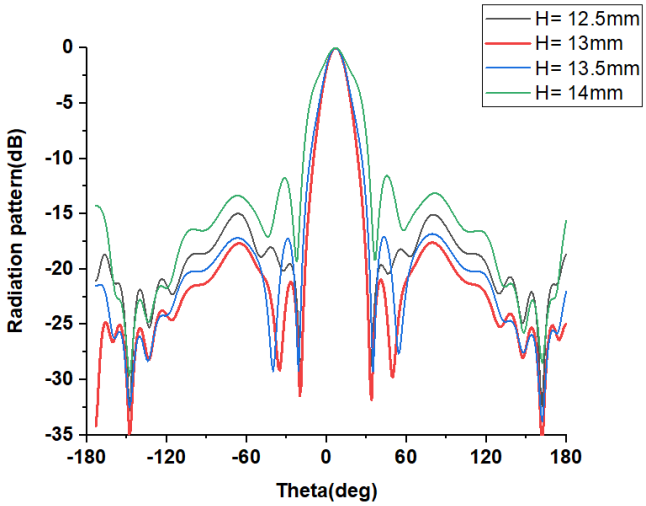

Fig. 7. Radiation patterns for different air cavity heights.

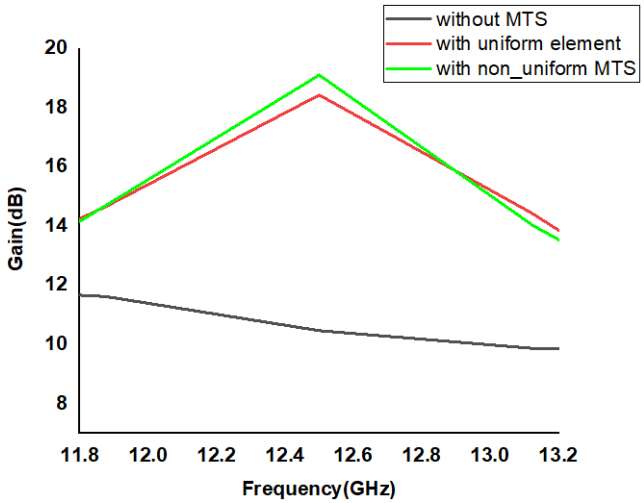

Fig. 8. Peak gain of the antenna without a metasurface, with a uniform metasurface, and with a non-uniform metasurface.

C. *Current Density Analysis*

Figure 9 depicts the current density on the metasurface with 11 × 11 uniform unit cells. The high central current density observed in Figure 9, emphasizes radiation along the boresight (normal to the metasurface), whereas the decreased current at the edges reduces contributions to grating lobes (Figure 11). The current is high at the center but decreases gradually towards the edges. The high current density at the center of the metasurface leads to high electromagnetic field contributions from the central unit cells, which enhances the overall gain from 10.3 dB to 17.5 dB and the directivity of the antenna system due to the tapered current distribution on the metasurface. The introduction of non-uniform unit cells enhances current concentration at the center by reducing the size of edge unit cells. Secondary electromagnetic fields produced by this current tapering influence the multiple reflections of the incident wave. Guided by current density analysis showing high central density decreasing toward the edges (Figure 10), this results in a gain enhancement of 1.1 dB

by further focusing energy in the main beam. The reduction of unit cell size at the edges introduces phase variation, which disrupts periodicity and enables the lowest grating-lobe levels of –20.22 dB (Figure 11).

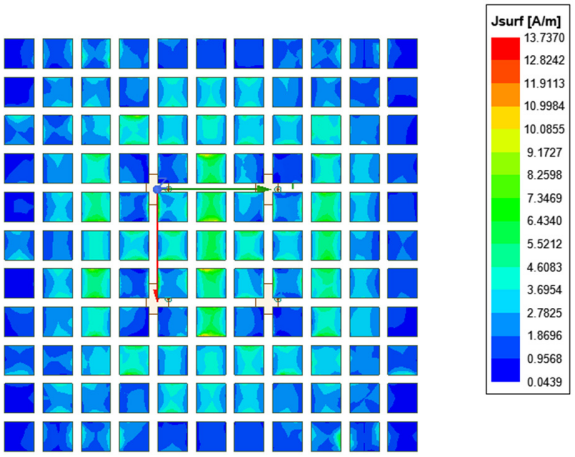

Fig. 9. Current density distribution with a uniform metasurface.

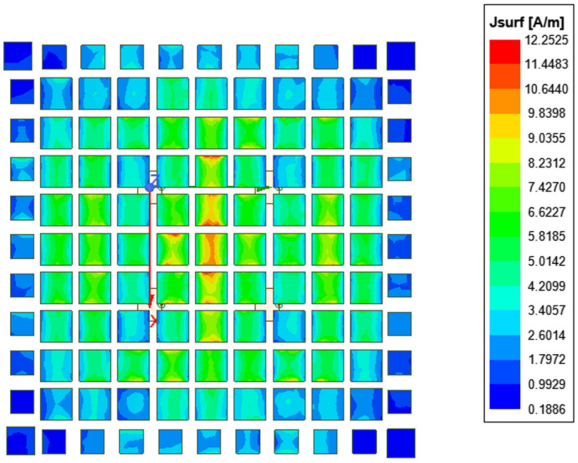

Fig. 10. Current density distribution with a non-uniform metasurface.

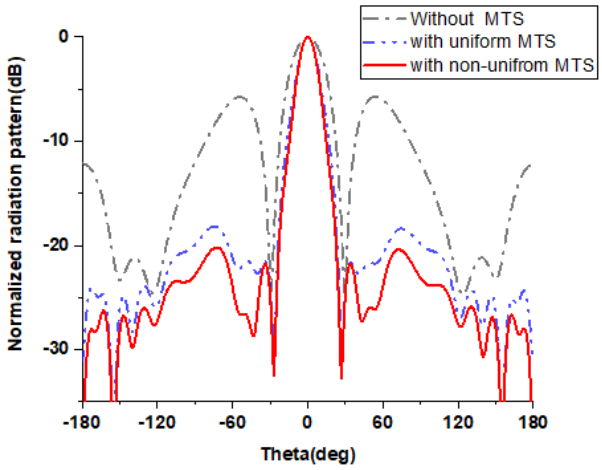

Fig. 11. Radiation patterns for the antenna without metasurface, with a uniform metasurface, and with a non-uniform metasurface.

V. DISCUSSION

The integration of a non-uniform metasurface-based PRS with a 2 × 2 microstrip patch antenna array with element spacing of 25 mm (1.04 λ_0), in an FPC configuration, demonstrates a robust solution for grating-lobe suppression and gain enhancement. The achieved GLL of –20.22 dB and a peak gain of 19.1 dB highlight the effectiveness of the proposed design. A cavity height of 13 mm, determined through parametric sweeps, minimized grating lobes to –18.5 dB, whereas the non-uniform metasurface with reduced edge unit cell sizes further lowered them to –20.22 dB, adding 1.1 dB to the gain. This improvement is due to the high central current density decreasing toward the edges, which focuses energy in the main lobe and disrupts the periodicity that causes grating lobes, as depicted in Figures 9–11.

The reflection amplitude of 0.85 and phase of −152.5° of the metasurface unit cells enhance the resonant cavity effect by facilitating constructive interference, whereas the near 180° phase shift aligns the reflected waves for boresight radiation, narrowing the beam and reducing sidelobes. This is consistent with the theoretical expectation that a phase close to −180°, combined with an optimal cavity spacing (i.e., $\lambda_0/2$), maximizes directivity.

Additionally, the proposed design achieves a gain of more than 15 dB over the frequency range 12–13.2 GHz, demonstrating stable and broadband performance. The E-plane and H-plane radiation patterns, presented in Figure 12, show that the grating lobes reach a maximum level of less than −20.22 dB in the H-plane and more than −15 dB in the E-plane, indicating great lobe suppression in both principal planes. Furthermore, the cross-polarization level in the H-plane remains below −25 dB. These results confirm that the non-uniform metasurface superstrate not only enhances the overall gain but also provides effective grating-lobe suppression. The non-uniform edge design, inspired by the observed current density taper, offers a novel approach, distinguishing this work from uniform metasurface designs.

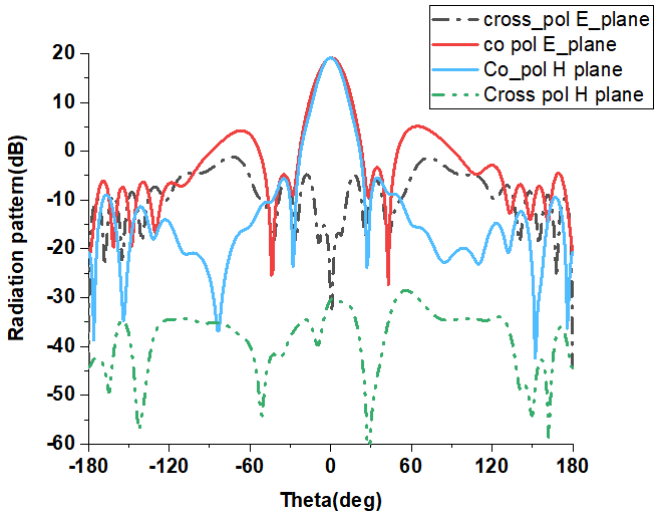

Fig. 12. Co-polarization and cross-polarization of the antenna for different configurations in the E-plane and H-plane.

A. Sensitivity Analysis

To assess robustness, a sensitivity analysis was performed by evaluating performance under ±5% variations in substrate permittivity ($\varepsilon_r = 4.4$), unit cell element spacing size ($l = 6.75$ mm), and cavity height ($H = 13$ mm). The results in Table I show that the GLL remains below –20 dB and the gain is maintained around 19 dB, confirming tolerance to fabrication errors. This simulation-based study, due to limited access to millimeter-wave fabrication facilities, provides a foundation for future experimental validation.

TABLE I. SENSITIVITY ANALYSIS

Parameter	Variation (mm)	GLL (dB)	Gain (dB)
Unit cell element spacing	7.83–8.66	–20 to –20.22	18.8–19.1
Unit cell size	6.4–7	–20.1 to –20.19	18.5–19.1
Cavity height	12.35–13.65	–20.01 to –20.2	17–19.09

B. Comparison with Related Works

Table II presents a summary of performance comparison between the proposed design and other related works. The studies were selected based on their relevance to large-element-spacing phased arrays, grating lobe suppression using metasurfaces or cavity-type approaches, and design complexity. This is important because these studies are similar in array configuration, employing FSS or PRS superstrates or metasurfaces, and represent the state-of-the-art in low-profile, high-gain antenna design. Therefore, they are appropriate for the assessment of the novelty and abilities of the proposed method.

TABLE II. COMPARISON OF THE PROPOSED WORK WITH REFERENCE STUDIES

Ref	Method	Array size	Element spacing	GLL (dB)	Design complexity
[6]	Aperiodic linear array	N/A	0.95/ $1.36\lambda_0$	–13	High
[9]	FPC electrically large property	2 × 2	$1.47\lambda_0$	–15.5	Moderate
[11]	PRS and AMC walls	1 × 1	2λ	–14.02	High
[12]	PRS and nonstandard AMC	2 × 2	2λ	–11	Moderate
[13]	PRS and filtering properties by a leaky-wave cavity in the far field	7 × 7	2λ	–19.31	High
[14]	Leaky-wave cavity with dielectric layers	11 × 11	1.5λ	–10	High
[10]	Multilayer FSS	8× 8	$1\lambda_0$	–10	High
[18]	Fabry–Perot metasurface lens	4 × 4	$1.5\lambda_0$	–16	Moderate
Our work	FPC with non-uniform metasurface	2 × 2	$1.04\lambda_0$	–20.22	Low

Unlike e.g. the work presented in [6], which employed a genetic algorithm over a large aperiodic array, the proposed structure achieves grating-lobe suppression without the need for complex optimization. Compared to the FPC design in [9], which demonstrated a GLL of –15.5 dB, the proposed design achieves –20.22 dB suppression with a simpler 2 × 2 antenna array configuration.

Approaches using AMC walls [11, 12] or PRS-based thinned arrays [13] can achieve notable improvements, yet they often rely on specialized reflective grounds or leaky-wave effects, adding structural or fabrication complexity. Similarly, dielectric superlayers [14] and multilayer FSS structures [10] reduce grating lobes but at the expense of bulky profiles and challenging implementations. Even metasurface lens solutions [18], though effective in enhancing gain and controlling lobes, tend to increase volume and design overhead.

The proposed non-uniform metasurface superstrate achieves the lowest reported GLL (–20.22 dB) in a compact, single-layer structure while simultaneously enhancing gain to 19.1 dB. This balance of low complexity, high suppression, and robustness positions the design as a practical and efficient alternative, particularly for size-constrained applications such as 5G base stations, radar, and satellite systems.

VI. CONCLUSION

This study successfully demonstrates the effectiveness of a novel non-uniform metasurface-based Partially Reflective Surface (PRS) integrated with a 2 × 2 microstrip patch antenna array, addressing grating-lobe issues and enhancing performance at 12.5 GHz. The optimized Fabry–Perot Cavity (FPC) height, combined with unit cell spacing, achieves a Grating Lobe Level (GLL) of –20.22 dB and a peak gain of 19.1 dB, supported by the high central current density tapering toward the edges. The reflection amplitude of 0.86 and phase near -180°, tuned via simulations in the High-Frequency Structure Simulator (HFSS), validate the FPC's role in focusing the main beam. Sensitivity analysis further confirms resilience to fabrication variations.

Compared to complex methods such as genetic algorithms or bulky multilayer Frequency Selective Surface (FSS) designs, the proposed approach achieves low profile, high grating-lobe suppression, and robust performance, making it ideal for 5G base stations, radar, and satellite applications. Future work on tunable metasurfaces is expected to further enhance adaptability, strengthening the practical impact of this design.

ACKNOWLEDGMENT

This research was carried out with the support of the Pan African University Institute for Basic Sciences, Technology and Innovation (PAUSTI).

REFERENCES

[1] Z. Iqbal and M. Pour, "Grating Lobe Mitigation in Scanning Planar Phased Array Antennas," in *2019 IEEE International Symposium on Phased Array System & Technology*, Waltham, MA, USA, 2019, pp. 1–3, https://doi.org/10.1109/PAST43306.2019.9020996.

[2] R. J. Mailloux, *Phased Array Antenna Handbook*, 3rd ed. Norwood, MA, USA: Artech House, Inc., 2017.

[3] S. Fang, Z. Xue, W. Li, and W. Ren, "Grating Lobe Suppression of Planar Array with Large Inter-Element Spacing by Using Genetic Algorithm," in *2018 International Conference on Microwave and*

Millimeter Wave Technology, Chengdu, China, 2018, pp. 1–3, https://doi.org/10.1109/ICMMT.2018.8563842.

[4] G. Tashtarian and M. S. Majedi, "Grating Lobes Reduction in Linear Arrays Composed of Subarrays Using PSO," in *2019 International Symposium on Networks, Computers and Communications*, Istanbul, Turkey, 2019, pp. 1–6, https://doi.org/10.1109/ISNCC.2019.8909108.

[5] X. Xu, C. Liao, L. Zhou, and F. Peng, "Grating Lobe Suppression of Non-Uniform Arrays Based on Position Gradient and Sigmoid Function," *IEEE Access*, vol. 7, pp. 106407–106416, 2019, https://doi.org/10.1109/ACCESS.2019.2932123.

[6] S. Suarez, G. Leon Fernandez, M. Arrebola, L. F. Herran Ontanon, and F. Las-Heras Andres, "Experimental Validation of Linear Aperiodic Array for Grating Lobe Suppression," *Progress In Electromagnetics Research C*, vol. 26, pp. 193–203, 2012, https://doi.org/10.2528/PIERC11110706.

[7] Y. Zhang *et al.*, "High-Gain Circularly Polarized Array Antenna With Low Grating Lobe Property Based on TM30/TM03 Mode," *IEEE Antennas and Wireless Propagation Letters*, vol. 20, no. 3, pp. 401–405, Mar. 2021, https://doi.org/10.1109/LAWP.2021.3052915.

[8] Y. Zhang, W. Cao, Z. Qian, S. Shi, and W. Peng, "Low Grating Lobe Array Antenna With Electrically Large Property Based on TM50 Mode," *IEEE Access*, vol. 7, pp. 32897–32906, 2019, https://doi.org/10.1109/ACCESS.2019.2903169.

[9] Y. Zhang, W. Cao, Z. Qian, and T. Pan, "High Gain and Low Grating Lobe Electrically Large Array Antenna by Using Fabry-Perot Cavity," *IEEE Access*, vol. 7, pp. 108677–108683, 2019, https://doi.org/10.1109/ACCESS.2019.2933404.

[10] J. R. Kelly and A. P. Feresidis, "Array Antenna With Increased Element Separation Based on a Fabry–PÉrot Resonant Cavity With AMC Walls," *IEEE Transactions on Antennas and Propagation*, vol. 57, no. 3, pp. 682–687, Mar. 2009, https://doi.org/10.1109/TAP.2009.2013429.

[11] Z.-G. Liu and W.-B. Lu, "Low-Profile Design of Broadband High Gain Circularly Polarized Fabry-Perot Resonator Antenna and its Array with Linearly Polarized Feed," *IEEE Access*, vol. 5, pp. 7164–7172, 2017, https://doi.org/10.1109/ACCESS.2017.2675378.

[12] D. Blanco, E. Rajo-Iglesias, A. Montesano Benito, and N. Llombart, "Leaky-Wave Thinned Phased Array in PCB Technology for Telecommunication Applications," *IEEE Transactions on Antennas and Propagation*, vol. 64, no. 10, pp. 4288–4296, Oct. 2016, https://doi.org/10.1109/TAP.2016.2597642.

[13] D. Blanco, N. Llombart, and E. Rajo-Iglesias, "On the Use of Leaky Wave Phased Arrays for the Reduction of the Grating Lobe Level," *IEEE Transactions on Antennas and Propagation*, vol. 62, no. 4, pp. 1789–1795, Apr. 2014, https://doi.org/10.1109/TAP.2013.2272573.

[14] D. Sánchez-Escuderos, M. Ferrando-Rocher, J. I. Herranz-Herruzo, and A. Valero-Nogueira, "Grating Lobes Reduction Using a Multilayer Frequency Selective Surface on a Dual-Polarized Aperture Array Antenna in Ka-Band," *IEEE Access*, vol. 8, pp. 104977–104984, 2020, https://doi.org/10.1109/ACCESS.2020.3000069.

[15] K. C. Rao, D. Nataraj, K. S. Chakradhar, G. V. Ujwala, M. Lakshmunaidu, and H. S. Dadi, "Design of a Compact Millimeter Wave Antenna for 5G Applications based on Meta Surface Luneburg Lens," *Engineering, Technology & Applied Science Research*, vol. 15, no. 2, pp. 20722–20728, Apr. 2025, https://doi.org/10.48084/etasr.9349.

[16] Z. Wang, Q. Liu, M. Yan, J. Liang, and D. Zhou, "Double-layer broadband transmission metasurface and its application in low sidelobe antenna," *Journal of Physics D: Applied Physics*, vol. 56, no. 19, Mar. 2023, Art. no. 195101, https://doi.org/10.1088/1361-6463/acc40d.

[17] F. Xue, S. Liu, and X. Kong, "Single-layer high-gain flat lens antenna based on the focusing gradient metasurface," *International Journal of RF and Microwave Computer-Aided Engineering*, vol. 30, no. 6, May 2020, Art. no. e22183, https://doi.org/10.1002/mmce.22183.

[18] Z. Wang *et al.*, "Unlock the Potentials of Large-Element-Spacing Arrays: A Meta-Lens Solution for Grating-Lobe Suppression and Gain Enhancement," *Electromagnetic Science*, vol. 2, no. 4, pp. 1–15, Dec. 2024, https://doi.org/10.23919/emsci.2024.0030.

[19] H. Zhu, Y. Cao, and G. Wei, "Study on Non-uniform Meta-surface for Antenna Design," in *2018 IEEE International Conference on Signal Processing, Communications and Computing*, Qingdao, China, 2018, pp. 1–4, https://doi.org/10.1109/ICSPCC.2018.8567722.

[20] S. Kruk and Y. Kivshar, "Tailoring transmission and reflection with metasurfaces," in *Dielectric Metamaterials*, I. Brener, S. Liu, I. Staude, J. Valentine, and C. Holloway, Eds. Sawston, Cambridge, UK: Woodhead Publishing, 2020, pp. 145–174, https://doi.org/10.1016/B978-0-08-102403-4.00010-4.

[21] Q. Zheng *et al.*, "Ultra-wideband side-lobe level suppression using amplitude-adjustable metasurfaces," *Journal of Physics D: Applied Physics*, vol. 52, no. 6, Dec. 2018, Art. no. 065102, https://doi.org/10.1088/1361-6463/aaf248.

[22] H.-P. Li, G.-M. Wang, T. Cai, J.-G. Liang, and X.-J. Gao, "Phase- and Amplitude-Control Metasurfaces for Antenna Main-Lobe and Sidelobe Manipulations," *IEEE Transactions on Antennas and Propagation*, vol. 66, no. 10, pp. 5121–5129, Oct. 2018, https://doi.org/10.1109/TAP.2018.2858181.

[23] F. Francis, S. Imaculate Rosaline, and R. Suresh Kumar, "A broadband metamaterial superstrate based MIMO antenna array for sub-6 GHz wireless applications," *AEU - International Journal of Electronics and Communications*, vol. 173, Jan. 2024, Art. no. 155015, https://doi.org/10.1016/j.aeue.2023.155015.